White Rose Research Online

eprints@whiterose.ac.uk
https://eprints.whiterose.ac.uk
Universities of Leeds, Sheffield and York

Deposited via The University of Sheffield.

White Rose Research Online URL for this paper:
https://eprints.whiterose.ac.uk/id/eprint/171285/

Version: Published Version

Article:
Zhang, Z., Hu, Y., Chen, X. et al. (2021) A review on conductive common-mode EMI suppression methods in inverter fed motor drives. IEEE Access, 9. pp. 18345-18360. ISSN: 2169-3536

https://doi.org/10.1109/access.2021.3054514

Reuse
This article is distributed under the terms of the Creative Commons Attribution (CC BY) licence. This licence allows you to distribute, remix, tweak, and build upon the work, even commercially, as long as you credit the authors for the original work. More information and the full terms of the licence here: https://creativecommons.org/licenses/

Takedown
If you consider content in White Rose Research Online to be in breach of UK law, please notify us by emailing eprints@whiterose.ac.uk including the URL of the record and the reason for the withdrawal request.

UNIVERSITY OF LEEDS
University of Sheffield
UNIVERSITY of York

IEEE Access
Multidisciplinary ⋮ Rapid Review ⋮ Open Access Journal

Received January 6, 2021, accepted January 20, 2021, date of publication January 25, 2021, date of current version February 1, 2021.

Digital Object Identifier 10.1109/ACCESS.2021.3054514

A Review on Conductive Common-Mode EMI Suppression Methods in Inverter Fed Motor Drives

ZELIANG ZHANG[1], YIHUA HU[1], (Senior Member, IEEE), XIAO CHEN[2], (Member, IEEE), GERAINT WYN JEWELL[2], AND HONG LI[3], (Senior Member, IEEE)

[1]Department of Electronics Engineering, University of York, York YO10 5DD, U.K.
[2]Department of Electronic and Electrical Engineering, The University of Sheffield, Sheffield S10 4DE, U.K.
[3]School of Electrical Engineering, Beijing Jiaotong University, Beijing 100044, China

Corresponding author: Yihua Hu (yihua.hu@york.ac.uk)

This work was supported in part by the Royal Society Industry Fellowship (INF\R1\201021) and in part by the Royal Academy of Engineering: Transforming Systems through Partnership (China).

ABSTRACT The impact of electromagnetic interference (EMI) is an increasingly important aspect of the performance of switching inverters. The challenges of managing EMI continue to grow with the emergence of wide bandgap (WBG) devices, the trend towards ever-greater integration and higher power rating. This paper reviews suppression methods for the conductive common-mode (CM) EMI in inverter fed motor drives. In order to span EMI suppression across the full system design process, the review considers both mitigation from the sources and suppression along the conduction paths. Furthermore, the shortcomings and merits of the reviewed publications are discussed, and their attenuation frequency range and attenuation level are compared. It is demonstrated that the CM EMI at low frequency is mainly determined by the PWM strategies and can be reduced or even theoretically eliminated through zero common-mode control. On the other hand, the CM EMI at high frequency is markedly influenced by the switching transients of the power devices. Thus, various drive circuits are reviewed which improve the switching behavior. Finally, the deployment of passive and active filters to suppress or compensate for the EMI is discussed.

INDEX TERMS Conductive EMI, EMI sources, inverter fed motor drives, propagation paths.

I. INTRODUCTION

Electric drives have been increasingly adopted in many industrial sectors due to their ability to yield highly controllable, fast response and high-power density systems solutions. However, as the switching frequency and switching speed of power devices and the inverter power continue to increase, the problems posed by Electromagnetic Interference (EMI) in electric drives are exacerbated. EMI has the potential to cause deterioration in the performance of electrical machines and its drive system through a variety of failure mechanisms, including, inter-alia, bearings damage, unexpected actions of power devices, interference on analogue feedback signals, etc. These problems eventually lead to system performance degradation or even shutdown.

EMI in electric drives can be classified as conductive EMI and radiated EMI. The conductive EMI is defined with the frequency range from 150 kHz to 30 MHz in standard DO 160 [1]. In accordance with different applications of motor drives, various standards on EMI measurement setup and EMI limits have been published and been revised over years, such as aeronautic standard DO 160 [1], Industrial Scientific and Medical (ISM) standard CISPR 11 [2] and CISPR 22/32 [3], military standard MIL-STD-461 [4], etc.

Accounting for different conductive paths, conductive EMI can be divided into differential-mode (DM) EMI and common-mode (CM) EMI. DM EMI is caused by the voltage differences between phases and results in conduction between the three phases. CM EMI is caused by the common-mode voltage (CMV), which can be defined as the voltage potential relative to a common reference point. In an inverter-fed motor system, the common reference point can be the earth O. The CMV of each phase is the voltage pulse between the phase input and O, and can be expressed as V_{AO}, V_{BO}, V_{CO} in a three-phase system. The voltage pulses have the same pattern as the driving signal of the upper-leg devices, but their amplitudes can be as high as the V_{DC}. In a traditional three-phase inverter, the average output CMV is defined as

The associate editor coordinating the review of this manuscript and approving it for publication was Inam Nutkani.

This work is licensed under a Creative Commons Attribution 4.0 License. For more information, see https://creativecommons.org/licenses/by/4.0/

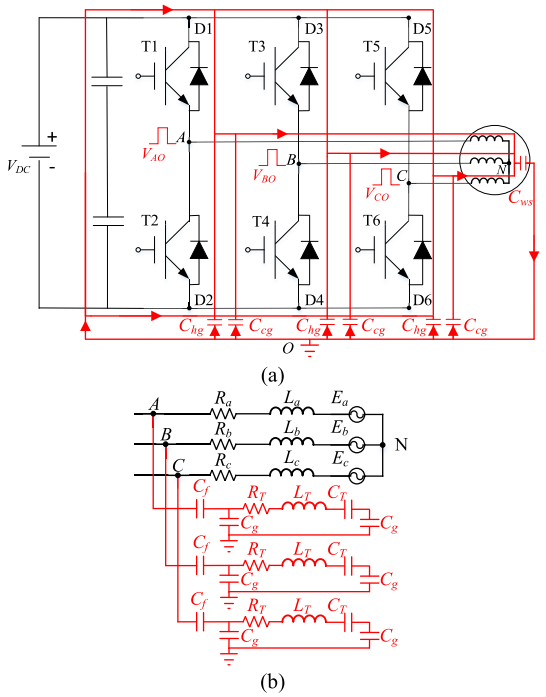

FIGURE 1. The main conduction paths of CM EMI in motor drives.

the voltage potential between the neutral point N and O and can be expressed as $V_{CM} = (V_{AO} + V_{BO} + V_{CO})/3$. The rapid CM voltage pulses are coupled to the earth through the parasitic components, resulting in high-frequency CM current, and finally produce interference on other components of the system. The main CM path in a typical three-phase voltage source inverter is shown in Fig. 1(a).

As depicted in Fig. 1(a), the parasitic components in drives form the various CM conductive paths. C_{ws} represents the parasitic capacitance between the motor winding and the grounded motor frame, while C_{hg} and C_{cg} stand for the heatsink to ground capacitance and cable to ground capacitance, respectively. Furthermore, the CM EMI conduction paths in windings are presented in Fig. 1(b), in which R_a, R_b, R_c, L_a, L_b, L_c, E_a, E_b, E_c represent the resistance, inductance and back EMF of each phase, while C_f blocks the fundamental frequency components, R_T, L_T, C_T stand for the interturn effect, and C_g represents the winding to ground capacitance. The magnitude of the capacitances encountered between various components in electrical machines and their drives has been modeled and measured in several publications, including the machine winding to frame capacitances in the context of bearing currents [5]–[7], power cable to cable capacitances [8] [9], power module internal capacitances [10], [11], and power module to heatsink capacitances [12]–[14]. These capacitances tend to have values in a range from 10pF to 1000pF.

The EMI sources in inverter fed motor drives predominantly comprise two elements, viz. the CMV caused by the discrete voltages generated by the inverter and the PWM; the high dV/dt and di/dt generated during the switching transient of power devices. The spectral distributions of EMI caused by the PWM sequences and switching transient of power devices are analyzed in detail in [15]. The result therein indicates that the EMI between 150 kHz to 5 MHz is determined mainly by the PWM sequences, while the switching transient influences the EMI between 5 MHz to 30 MHz. On the one hand, the harmonics of discrete output voltage induces ripple current at low frequency. On the other hand, due to the rapid switching actions of the power devices, the high dV/dt induces large charging/discharging currents in parasitic capacitances at high frequency. The higher the switching frequency and DC bus voltage of the inverter, the more problematic the EMI caused by the inverter is likely to be.

There are two main research topics on conductive EMI, viz., conductive EMI suppression and the development of high-frequency models of conduction paths of EMI. Establishing high-frequency models aims to intrinsically suppress conducted EMI better, for example, optimizing the design of EMI filters based on high-frequency models. Several review papers have been published on these two topics. In [16], S. Wang *et al.* review the advances in EMI modeling techniques for adjustable speed drives. The equivalent circuits for high-frequency models of induction machines and rectifier-inverters are presented.

Although EMI suppression is discussed in [16], only EMI filters and reduced CMV PWM techniques are explored. The EMI characteristics and EMI reduction methods for wide bandgap (WBG) devices are reviewed in [17]. However, [17] mainly focuses on the reduction methods based on the power devices, such as advanced gate drive and packaging optimization. Furthermore, in [18], A. Amin and S. Choi also pay their attention to WBG devices and emphasize the role of passive filters and active filters in EMI reduction. In [19], EMI reduction methods for DC-DC converters are discussed, but zero CMV techniques are not included. Collectively, these review papers are somewhat lacking in quantitative analysis and arguably do not comprehensively review the full spectrum of EMI reduction methods for inverter fed drives.

This paper aims to review the existing CM EMI reduction methods that can be adopted at either the early stage or the later stages of the machine drive design process. At the early stage, the EMI can be suppressed from its sources while at the later stages, filters can be applied to attenuate the EMI along conductive paths. Hence, the reviewed publications are categorized into two classes as shown schematically in Fig. 2. For each publication reviewed, the effective frequency range and reduction effects are summarized. In section II, methods employed for mitigating EMI from sources are presented. The methods that are able to suppress EMI along conductive paths are presented in section III. In section II and section III, the principles and status of each method are presented. In section IV, the attenuation frequency range and attenuation level provided by each method are compared. The merits and drawbacks and likely future trends in the development of EMI suppression methods are discussed in section IV. Section V draws key conclusions from the review.

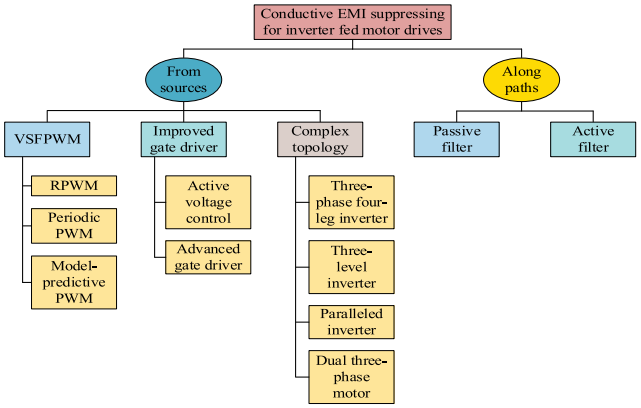

FIGURE 2. Categorization of main research topics on EMI reduction for inverter fed motor drive.

II. EMI MITIGATION FROM EMI SOURCES

From the perspective of EMI sources, EMI mitigation can be achieved by applying variable switching frequency PWM (VSFPWM) and improving the switching transient of power devices. Besides, although the CMV of three-phase two-level switching inverters cannot be eliminated, complex topologies of inverters and motors developed in recent years provide options for theoretically eliminating CMV.

A. VARIABLE SWITCHING FREQUENCY MODULATION STRATEGIES

Constant switching frequency PWM(CSFPWM), such as space-vector PWM (SVPWM), has been widely applied in conventional inverter control strategies. The harmonics of voltage and current are concentrated at integer multiples of the switching frequency under CSFPWM. These concentrated harmonics generate EMI at low frequency, i.e., tens to hundreds of kHz.

To reduce EMI peaks at the switching frequency and its integer multiples, spread spectrum modulation strategies have been introduced to achieve VSFPWM. VSFPWM spreads the concentrated harmonics over a wider frequency band, which has the effect of reducing EMI peaks. According to different means of varying the switching frequency, VSFPWM applied in motor drives can be classified as random switching frequency PWM (RSFPWM), periodic PWM, and model predictive PWM. By way of illustration, Fig. 3 compares representative current harmonic magnitude patterns of RSFPWM, periodic PWM and model-predictive PWM against CSFPWM. Fundamentals are excluded in Fig. 3, and f_{c0} denotes the carrier frequency.

RSFPWM controls the switching frequency varying randomly on both sides of the constant switching frequency. Assuming the constant switching frequency of the inverter is $f_c(t_0)$, $Rand \in(-1,1)$ is a random number, $\theta \in(0,1)$ is a constant coefficient, the switching frequency f_c of RSFPWM can be expressed as $f_c = f_c(t_0) \times (Rand \times \theta)$. The generation of pseudo-random signals and SVPWM were implemented on an FPGA-based electric drive in [20], which demonstrated that RSFPWM can spread the spikes

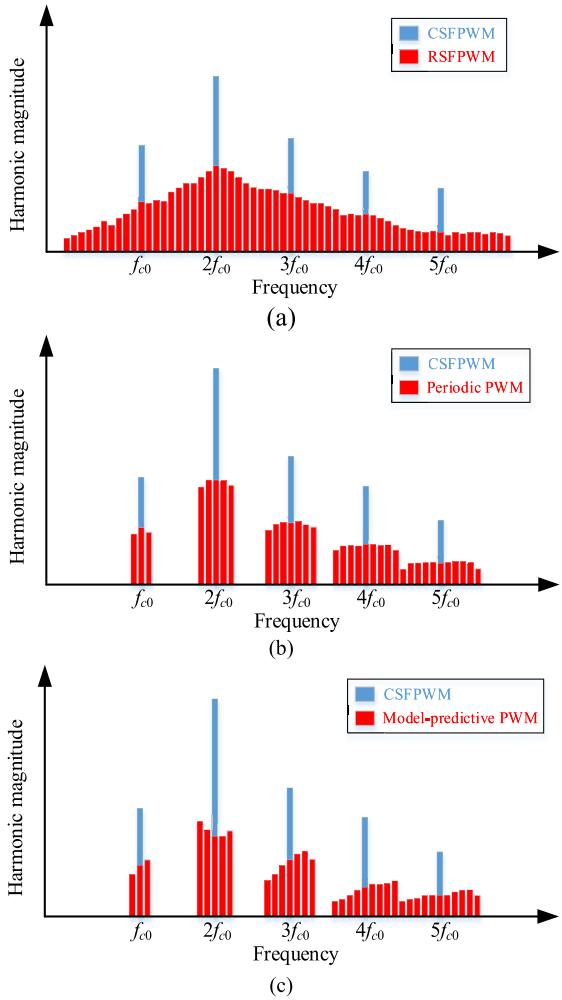

FIGURE 3. Comparison of representative current harmonic magnitude patterns of variable switching frequency PWM and constant switching frequency PWM. (a) RSFPWM vs CSFPWM. (b) Periodic PWM vs CSFPWM. (c) Model-predictive PWM vs CSFPWM.

of line voltage harmonics to nearby frequencies. For the purpose of enhancing the harmonic power spreading ability of RSFPWM, multiple carriers based RSFPWM is proposed in [21] to improve the randomness of the switching frequency. In [22], due to the excellent performance of RSFPWM in reducing harmonic peaks, RSFPWM is introduced to interior permanent magnet synchronous machine (IPMSM) sensorless control based on high-frequency signal injection to spread out the additional harmonics, yielding a 20dB attenuation in the power peak of full-spectrum. The voltage, current, and acoustic noise spectral characteristics of five state-of-the-art RSFPWM strategies in adjustable-speed drives (ASD) are quantitatively evaluated in [23], and the experimental results demonstrate that RSFPWM can attenuate the acoustic noise peaks by more than 20dB in an induction motor drive. These RSFPWM publications focus mainly on noise reduction rather than EMI suppression. In [24], the EMI spectrum of RSFPWM is analyzed in-depth, indicating that RSFPWM can eliminate discrete common-mode voltage spikes in the

1-100kHz band. The randomness inherent in the switching frequency raises the following concerns:

a) The switching loss cannot be predicted as the switching frequency changes in a random manner, which makes efficiency calculation challenging. Hence, the thermal subsystem cannot be optimally designed [25];

b) RSFPWM cannot arrange the spectral distribution of harmonic energies, and it is not effective in suppressing specific harmonics;

c) In some applications, RPWM increases the requirements for EMI filters [24].

In contrast to RSFPWM, periodic PWM changes the switching frequency periodically within a certain range, and the switching frequency of periodic PWM can be expressed as: $f_c = f_c(t_0) + Func(t) \times \Delta f_c$, where $Func(t)$ indicates specific changing patterns and Δf_c is the varying width of the switching frequency. According to different frequency-changing patterns, periodic PWM can be classified as having a sinusoidal profile, exponential profile, triangular profile [26], [27], [27], or sawtooth pattern [29]. It is noted in [30] that the Δf_c is a key factor affecting the spreading effect of periodic PWM. EMI peaks decrease as Δf_c increases. However, when Δf_c increases to a certain degree, the overlapping of harmonics will occur, which acts to counter the suppression of EMI. In [29] [31], Y. Xu *et al.* conducted a comparative study on inverter loss and motor loss in PMSM drives using CSFPWM, sinusoidal periodic PWM, and sawtooth periodic PWM, demonstrating that periodic PWM does not increase inverter loss, but it will marginally increase motor loss compared to CSFPWM. Furthermore, in [32], it is demonstrated that in the frequency band between 1 kHz to 100 kHz, sawtooth periodic PWM has a superior ability to suppress common-mode conducted EMI than sinusoidal periodic PWM. Since the switching frequency of periodic PWM varies periodically, inverter loss prediction can be performed to improve efficiency and optimize thermal design.

RSFPWM and periodic PWM achieve the effect of reducing the values of EMI spectrum peaks by changing the switching frequency within a certain range. However, these two modulation strategies are the direct application of spread spectrum modulation strategies in inverters, and the changes on the switching frequency of inverters are not calculated theoretically and lack an underpinning analytical basis.

To precisely control the current ripple caused by different switching strategies, in [33], [34], D. Jiang and F. Wang *et al.* presented two VSFPWM strategies based on current ripple prediction. An analytical model is developed to predict three-phase current ripple using the switching frequency and PWM duty ratio. The switching frequency is then adjusted to control the ripple to meet the desired ripple specification. Furthermore, in [35], the EMI mitigation effects of model predictive VSFPWM on AC motor drives are investigated.

It is can be seen that VSFPWM can realize the suppression of EMI at low-frequency without the need for additional hardware. Furthermore, the emergence and growing adoption of WBG devices brings the prospect of much higher switching frequencies, so that Δf_c can increase to further improve the spectral dispersion effect of VSFPWM on EMI spikes. The application cases, effective frequency and effects of variable switching frequency PWM are summarized in Table 1.

However, because of the relatively large duration of PWM sequences (typically tens to hundreds of milliseconds), VSFPWM tends to achieve limited suppression of EMI at high-frequency which is predominantly induced by the switching transients of power devices. To suppress conducted EMI at tens of MHz, it is necessary to ameliorate the switching transients, e.g. by adopting improved gate drive circuit.

B. IMPROVED GATE DRIVE CIRCUIT FOR POWER DEVICES

Compared with the tens to hundreds of milliseconds durations of typical PWM sequences, the time scale of switching transient of power devices lie in the range of tens to hundreds of nanoseconds depending on the devices and the gate driver. Therefore, during switching transients, the high *dV/dt* and accompanying voltage ringing caused by impedance mismatch tend to worsen the EMI performance at high frequencies up to hundreds of MHz.

It is shown in [36] that the corner frequencies of the spectrum of EMI generated by power devices are determined by the duty ratio of the PWM sequence and the switching time, indicating that the device switching behavior has a significant impact on the EMI at high frequencies. The EMI at high frequencies can be suppressed by slowing switching transients, albeit at the expense of increased switching losses.

In [37], the switching losses and EMI of IGBTs are quantitatively compared for SiC devices and Si-SiC combination devices. In order to obtain the best trade-off between EMI suppression and switching loss, switching transient shaping based on active voltage control (AVC) and active gate driver (AGD) have attracted much research interest of late. Typical circuit schematics for implementing these two techniques are illustrated in Fig. 4.

AVC is a hardware-based solution for forcing the IGBT collector voltage (V_{ce}) transient to follow a predefined trajectory through feedback using quantities such as V_{ce}, V_{ge}, and *dV/dt*. X. Yang *et al.* proposed a method for controlling the switching transients of IGBT into Gaussian S shapes in [38] so that the discontinuities of PWM edges are eliminated due to the infinitely differentiable characteristics of Gaussian function, resulting in a significant reduction of EMI in the range 1-100MHz. Based on the Gaussian S-shaped IGBT switching transients, the analysis on the trade-off between switching losses and high-frequency EMI suppression is investigated in [39] using an accurate IGBT high-frequency model demonstrated in [40].

AGD is a gate driving circuit which adjusts the switching speed by controlling *dV/dt* and *di/dt*. Compared to AVC, AGD tends to introduce additional switching losses as a consequence of longer switching times. In [41], the gate driving circuit varies the gate drive voltage as different stages of switching transient, so as to exercise control over the

TABLE 1. Summary of variable switching frequency PWM method key findings.

Method	Ref.	Cases	Theme	Frequency of interest	Contribution
RSF PWM	[20]	VSI fed AC motor	Implementation of conventional RSFPWM	Below 150 kHz	Less than 5 dB attenuation on line voltage harmonic peaks compared with SVPWM
	[21]	VSI fed induction motor	To enhance the randomness, the random carrier is synthesized by four carriers of different frequencies	Below 150 kHz	Compared with conventional RSFPWM, harmonic spread factor of the output voltage is reduced by 21% while THD and PSD remains the same
	[22]	IPMSM sensorless control	Random frequencies for switching and HF signal are adopted to spread the power spectrum	Around the switching frequency	More than 20 dB/Hz attenuation on stator current PSD peaks
	[23]	VSI fed induction motor	A comparative study of 5 RPWM strategies under different fundamental frequencies	Below 50 kHz	Greater than 20 dB/Hz attenuation of PSD peaks of line voltage and phase current
	[24]	VSI fed induction motor	Frequency-domain and time-domain analysis of common-mode voltage	1 kHz to 100 kHz	Up to 4 dBμV and 11 dBμV reductions on peak and average values of CMV harmonics
Periodic PWM	[26-28]	Buck converter	Study on the EMI spectrum when the carrier frequency varies in sinusoidal, exponential and triangle profiles	150 kHz to 30 MHz	Approximately 20 dBμV reductions on the EMI peak values and these three modulation profiles show small differences
	[29][31]	VSI fed PMSM	Study on inverter losses and motor losses in PMSM drives using periodic PWM methods	Around the switching frequency	The periodic PWM does not increase inverter losses, but it will slightly increase motor losses
	[32]	VSI fed PMSM	A comparative study on EMI suppression abilities of periodic PWM modulated in sinusoidal and sawtooth profiles	Below 100 kHz	Sinusoidal and sawtooth profiles both bring more than 10 dBμV reductions on EMI peaks and have small differences
Model predictive PWM	[33][34]	Three-phase converter	Propose two model predictive PWM methods to reduce EMI and control the peak value and RMS value of current ripple	10 kHz to 1 MHz	These two methods bring 10 dBμA attenuation on EMI current and more than 10% reduction on switching losses
	[35]	Multi-level inverter fed PMSM	Apply model predictive PWM on AC motor drive to control the current ripple and EMI	10 kHz to 1 MHz	More than 10 dBμA attenuation on EMI current and about 33% reduction on switching losses

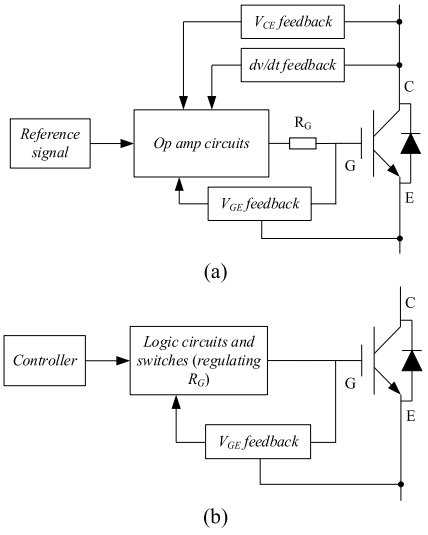

FIGURE 4. Schematics of the improved gate driver techniques. (a) AVC. (b) AGD.

switching speed. To further optimize the switching losses of IGBT caused by AGD, a digital active gate driver (DAGD) based on FPGA is designed and reported in [42] and [43]. Through the condition monitoring of the load current, the most appropriate parameters of the drive circuit are determined by an FPGA. Compared with AGD, switching losses can be significantly reduced (reducing by 42% in [42] and 64.7% in [43]) using DAGD, but at the expense of increased circuit complexity.

In comparison to more established Si-based switching device technologies, WBG devices can operate at higher switching frequency with low switching loss. However, WBG devices give rise to greater *di/dt* and *dV/dt* which make WBG devices not only the source of more severe conductive EMI, but also more likely to be affected by cross-talk between devices in the same leg. This cross-talk can lead to unexpected switching action and has the potential to cause the short-circuit failure or reverse breakdown. In [44], the mechanism and conduction path of crosstalk between two devices in the same leg is described, and a clamped circuit is proposed to eliminate any positive or negative spurious voltage caused by cross-talk. A summary of the requirements for the SiC drive circuits and the designed circuits to suppress crosstalk is presented in [45] and [46]. In [47] and [48], AGD is introduced into a SiC drive circuit to suppress overshoots by controlling the value of the gate resistor (R_g) during the Miller plateau effect. In [49] and [50], a logic circuit-based AGD is applied to dynamically adjust the effective value of R_g to achieve an improved trade-off between fast switching duration and suppressing voltage ringing. Instead of increasing the R_g to slow down the transient, in [51], the V_{gs} of the SiC MOSFET is adjusted using multiple power supplies.

TABLE 2. Summary of improved drive circuits key findings.

Method	Ref.	Cases	Theme	Frequency of interest	Contribution
Active voltage control	[37]	Single power device	Investigation on EMI and losses caused by switching transient of IGBT, SiC and Si-SiC	Up to 100 MHz	Compared with IGBTs, the high *dV/dt* of SiC incurs EMI increasing by maximum 30 dBμV
	[36]	IGBT	Compare S-shaped (twice differentiable) switching transient and trapezoidal (thrice differentiable) transient	Up to 100 MHz	S-shaped transient introduces an additional 20 dB/dec steeper gradient at high frequencies
	[38]	IGBT modules	Apply Gaussian switching transient (infinitely differentiable) on IGBT modules	1-100 MHz	The maximum EMI reduction goes to 40 dB and occurs between 10-20 MHz
Advanced gate drive	[41]	IGBT	Control the *dV/dt* and *di/dt* by setting different voltage levels of driving signal	-	The switching time is increased depend on different signal voltages so that the overshoot is suppressed
	[47][48]	SiC MOSFET	Change the gate resistance during the Miller plateau effect to suppress the overshoot and ringing	Up to 100 MHz	Voltage overshoots is reduced by 28% and the EMI noise with a resonant frequency of 5.4 MHz is eliminated
	[49][50]	SiC-based induction motor drive	In a switching duration, reduce the gate resistance at the start and end stages and increase the resistance at the middle stage	-	Voltage overshoots is reduced from 45% of the DC voltage to 5%
	[51]	SiC MOSFET	The AGD is fed by multiple power supplies, and these power supplies are selected by switches controlled by CPLD	Below 1 GHz	The AGD eliminates the noise in V_{ds} with resonant frequency of 9.2 MHz
	[52]	GaN MOSFET	A current mirror amplifying the feedback current is integrated with a push-pull buffer into an ASIC	Below 1 GHz	Compared with IGBTs, the high *dV/dt* of SiC incurs EMI increasing by maximum 30 dBμV
	[53]	GaN MOSFET	A programmable IC driver is designed to realize variable output resistance (R_g) with an ultra-high timing resolution	Below 2 GHz	S-shaped transient introduces an additional 20 dB/dec steeper gradient at high frequencies

In addition to adjusting R_g and V_{gs}, a current proportional to *dV/dt* is subtracted from the gate current (I_g) to reduce the *dV/dt* and switching loss of GaN transistors in a most recent study [52]. Due to the faster transient of GaN transistors, the AGDs applied on GaN transistors are required to achieve fast response. In [53], the R_g update rate achieves sub-nanosecond resolution (6.7 GHz).

As the two gate drive circuits shown previously in Figure 4, AGD can control the switching speed while it is unable to shape the switching transient. Hence, the optimal trade-off between switching loss and switching speed is more difficult to achieve in AGD compared with AVC, which is a voltage control system based on operational amplifiers. The features of reviewed papers on improved gate drive circuits are summarized in Table 2.

C. COMPLEX TOPOLOGIES OF INVERTER AND MACHINES

As previously discussed in Section I, at the CMV of conventional three-phase two-level inverters cannot be zero at any instant, and hence CM EMI cannot be eliminated in such inverters. To further reduce, or even eliminate, the CMV, a variety of modified, and in some cases complex, inverter and machine topologies has been developed to minimize the CMV. The topologies used to eliminate or mitigate EMI include three-phase four-leg inverters, three- level inverters, paralleled inverters, and dual three-phase motors. Schematics of these various arrangements are shown in Fig. 5.

The concept of a four-leg inverter is introduced to motor drives in [54]. Four *LC* passive filters are mounted at the output points of four legs to connected the fourth leg to the three-phase system, which introduces a negligible load unbalance. To eliminate the CMV, special modulation strategies need to be designed in which zero vectors (i.e. 000 and 111) are not permitted.

F. Lee *et al.* first proposed the concept of 3-Dimensional space vector modulation (3-D SVM) in [55] and [56]. 3-D SVM introduces the r-axis into α-β coordinates, so as to demonstrate the 16 switching states in 3-D α-β-r coordinate. The CMV can be eliminated when the inverter is operated with 6 switching states from among the total of 16 states. Hence, the SVPWM used in conventional inverters can be performed using the 6 zero CMV (ZCMV) space vectors. Although the CMV is eliminated, the number of optional space vectors decreases from 8 to 6, which reduces the utilization of the DC bus voltage.

A three-level inverter is combined with a four-leg inverter in [57]. The three-level inverter offers more options for avoiding zero vectors and does not reduce the utilization of DC voltage. The fourth leg can be used not only to eliminate the CMV, but also for fault-tolerant design of electric drives. In [58], the options provided by the fourth leg are fully utilized: the fourth leg is used to eliminate the CMV when the inverter is healthy, to operate fault-tolerant control when IGBT faults occur and to be operated as a boost converter during voltage sags.

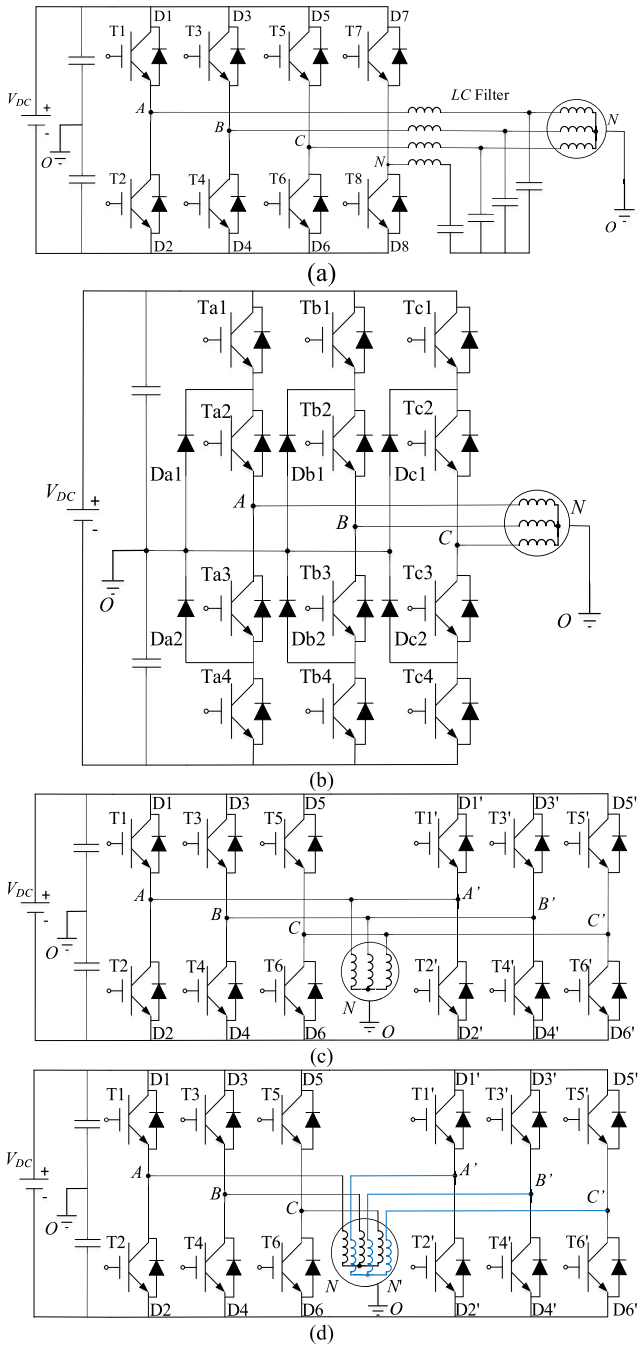

FIGURE 5. Schematics of modified topologies of inverter and machines. (a) Three-phase four-leg inverters. (b) Three-level inverters. (c) Paralleled inverters. (d) Dual three-phase motors.

In three-level inverters, the voltage between the mid-point of each phase and ground can take one of 3 values, viz. $\pm V_{DC}/2$ or 0. With the extra 0 level, 7 space voltage vectors can achieve ZCMV output among the total 27 space vectors of three-level inverters. H. Zhang *et al.* first realized the ZCMV PWM in [59]. However, implementing ZCMV modulation directly in three-level inverters deteriorates the performance of three-level inverters due to the constraint of avoiding zero vectors. Therefore, following the initial proposal of the concept of ZCMV PWM, many subsequent studies have focused on reducing the side effects caused by ZCMV PWM, such as increases in output voltage THD, current ripple, and switching loss. To reduce the switching loss, a three-segment switching sequences for zero CMV modulation is realized in [60]. To reduce the current ripple and THD, a four-state ZCMV PWM is presented in [61] with its four PWM sequences. According to synthesizing reference vectors with different space vectors, three types of ZCMV PWM for three-level inverters are listed and comparatively studied in [62]. In [63] and [64], VSFPWM is applied in three-level inverters to obtain an improved trade-off between EMI suppression and the performance of three-level inverters, albeit that CMV cannot be eliminated in this way.

In terms of EMI suppression, compared with four-leg inverters and three-level inverters, paralleled inverters not only have more options on achieving ZCMV PWM, but also are able to realize selected harmonics reduction by phase-shifting the carrier waves of the two paralleled inverters. The orders of the selected harmonics are dependent on the interleaving angle introduced by the carriers phase-shifting. In [65], harmonics in multiple orders are reduced through optimizing the interleaving angle, hence reducing the passive components of CM or DM EMI filters. However, the interleaving between two paralleled inverters also introduce CM and DM circulating current between two inverters. Therefore, inter-phase inductors are adopted to connect two inverters to limit the circulating current and are improved in [66] by optimizing the magnetic circuit to reduce its weight and volume. The effect of the interleaving angle between the carriers of two inverters on harmonic elimination is analyzed in [65]. Furthermore, in [67], carrier phase-shifting combined with discontinuous SVPWM is applied on a paralleled inverter to limit the CM circulating currents. Although the selected harmonics can be reduced or eliminated through carriers phase-shifting, CM voltage cannot be eliminated. As mentioned before, ZCMV PWM can also be implemented in paralleled inverter since paralleled inverters have even numbers of legs. The concept of paralleled space vectors is proposed in [68] and [69], with 6 paralleled space vectors explored to realize ZCMV PWM. In [70], a novel dual-segment three-phase PM machine is introduced to eliminate the need for the inter-phase inductors between two inverters, with consequent benefits in power density.

Dual three-phase arrangements proposed by H. Zhang achieves CMV cancellation utilizing two sets of symmetrical winding [71], [72]. The two sets of windings are directly paralleled without inter-phase inductors and are supplied by two inverters on a common DC bus. The CMVs of the two inverters have the same magnitude but opposite phases, so that the two voltages cancel each other, thereby achieving near ZCMV. In [73], ZCMV is achieved in an asymmetrical six-phase motor with interleaved windings by PWM signal shifting arrangement. Also, Carrier phase shifting [74], [75] and model predictive PWM [76] are applied on dual three-phase motors to improve the performance.

TABLE 3. Summary of complex topologies key findings.

Method	Ref.	Cases	Theme	Frequency of interest	Contribution
Three-phase four-leg inverter	[55][56]	Four-leg inverter with *LC* load	Proposes the concept of 3-D SVPWM to adapt the space vector modulation to three-phase four-leg inverter	-	The 3-D SVPWM provides 6 ZCMV vectors to realize ZCMV modulation
	[54]	Four-leg inverter fed Induction motor	Compares the CMV generated by the three-phase inverter, three-phase inverter with non-zero state modulation, and three-phase four-leg inverter	Up to 100 kHz	The fourth leg reduces CMV by 30 dB compared with three-phase inverter and reduces extra 20 dB above 60 kHz compared with three-phase inverter with non-zero state modulation
	[57]	Three-level four-leg inverter motor drive	Introduces the fourth leg to a three-level inverter, so as to obtain more ZCMV vectors	150 kHz to 10 MHz	attenuate the EMI by 20 dBμA across the all frequency range
	[58]	Four-leg inverter fed induction motor	Active zero state PWM is applied to eliminate the CMV generated by zero vectors	Up to 150 kHz	The RMS value of CMV and ground current is reduced by 60% and 80% respectively
Three-level inverter	[59]	Three-level inverter fed synchronous motor	First utilizing the 7 ZCMV vectors among the 27 vectors of three-level inverter to realize CMV control	Up to 20 kHz	The CMV is almost eliminated, but the THD of output line-to-line voltage is increased due to the ZCMV control
	[60]	Three-level inverter with *RL* load	Proposes 3-segment ZCMV switching sequences to reduce the switching commutation numbers	-	The switching commutation number is reduced by 50% without increases on the THD of output line-to-line voltage
	[61]	Three-level inverter fed induction motor	Proposes a four-state ZCMV PWM with its four sequences to reduce current ripple and THD	Integral multiples of switching frequency	The RMS value of current ripple is reduced from 0.131 A to 0.075 A, and the current THD is reduced by half
	[62]	Three-level inverter with *RLC* load	Compares three ZCMV PWM methods in terms of DC utilization, DC ripple, THD and power losses	-	The ZCMV PWM method which synthesizes reference vectors with 2 medium vectors and 1 zero vector performs better on all aspects
Paralleled inverter	[65]	Paralleled inverter with *RL* load	Discusses the effects of interleaving angle on reducing the output current ripple and the size of interphase inductors	Integral multiples of switching frequency	With 180° interleaving, the THD of ripple current and the weight of inductors can be reduced by 70% and 60% respectively
	[67]	Paralleled inverter with *RL* load	Eliminates the low-frequency CM circulating current by avoiding the coexistence of different zero vectors	-	The proposed PWM method can eliminate low-frequency CM current under symmetric or asymmetric interleaving
	[68][69]	Paralleled inverter with *RL* load	Propose paralleled voltage vectors to achieve ZCMV control	Up to 2 MHz	Greater than 20 dBμV EMI reduction compared with conventional SVPWM
	[70]	Paralleled inverter fed dual-three phase PMSM	Designs a special dual-segment PMSM to cancel the interphase inductors of paralleled inverter	150 kHz to 1 MHz	ZCMV PWM brings 10 dBμV reduction on peak EMI compared with conventional SVPWM
Dual three-phase motor	[71][72]	Dual-inverter fed dual three-phase motor	Two inverters generate reverse CMV to achieve ZCMV on the two sets of windings	Integral multiples of switching frequency	The leakage current to ground is reduced by more than 20 dB
	[73]	Dual-inverter fed dual three-phase motor	Proposes a ZCMV PWM scheme on asymmetrical six-phase PMSM based on PWM shifting	150 kHz to 2 MHz	The proposed PWM shifting ZCMV scheme brings 20 dB average peak EMI reduction comparing to SVPWM
	[76]	Dual-inverter fed dual three-phase PMSM	Propose a variable switching sequence PWM based on model predictive method to suppress current harmonics	Up to 10 MHz	Maximum 40 dBμA reduction on DC current EMI below 1 MHz

Although the use of complex topologies can, at least in principle, eliminate common-mode voltages, ZCMPWM will increase output ripple and harmonics, increase switching losses, and reduce bus voltage utilization. Therefore, in addition to ZCMPWM, the combination of advanced modulation strategies and complex topologies has become a research hotspot in recent years, in large part since this combination of approaches has the potential to achieve a good balance between EMI suppression and inverter performance. Table 3 summaries the reviewed publications on complex topologies of machines and inverters.

III. EMI SUPPRESSION ALONG PROPAGATION PATHS

The methods of suppressing EMI from sources are mainly adopted at the early stage of system design. However, for drives in which the EMI has not been fully mitigated at source

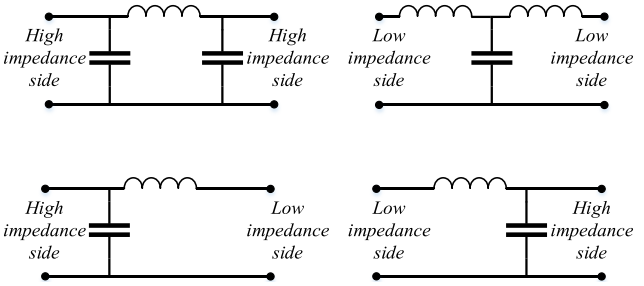

FIGURE 6. Illustration of impedance mismatch principle.

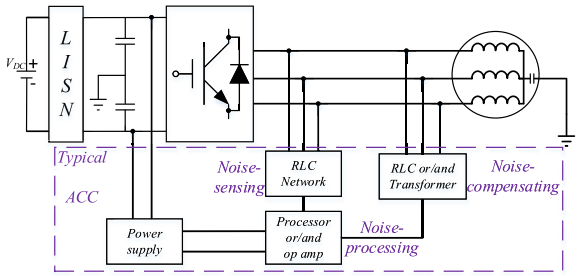

FIGURE 7. Schematic of the typical active EMI filter.

or drives that have already been designed and manufactured, EMI filters are often required to meet the often-stringent EMI requirement of the relevant standards. It is also worth noting that in some case, the environment into which the drive is integrated may require the adoption of additional filtering. EMI filters can be categorized into two types: passive filters and active filters. The advances in these two types of filters are reviewed in this section.

A. PASSIVE EMI FILTERS

Passive EMI filter is one of the most important and effective solutions to suppress conductive EMI. Inserting a filter at the input of inverters can improve the qualities of feedback signals while inserting a filter at the inverter output can reduce the three-phase current ripple, hence improving the overall performance of the motor drive.

Passive filters form resonant circuits in EMI propagation paths to reflect or shunt EMI currents. In practice, several filters can be cascaded to suppress EMI at different frequencies and enhance the insertion loss. There are several common filter configurations, including LC, CL, CLC, and LCL. For different source impedances and load impedances, suitable configurations should be selected according to the principle of impedance mismatch[77]. The preferred filter configurations involve connecting the inductances to the side with the lower series impedance and the capacitors to the side with higher parallel impedance, as shown in Fig. 6. In this way, the reflection coefficients of the transmission line are maximum to reflect EMI as much as possible.

H. Akagi *et al.* designed passive filters to suppress the leakage currents between inverter to the ground [78], [79], machine frame to the ground [78], [80], and the bearing current [81], so that the leakage currents and the bearing current were reduced by 90%. In [81], a line filter (DC side of the inverter) and machine filter (AC side of the inverter) are combined to attenuate the CM EMI. To explore the influence of different filter mounting positions, J. Xue and F. Wang compare the differences among EMI filters installed at the inverter output, motor input, and motor chassis in [82], discussing the application scenarios of the three installation methods. In [83] and [84], comprehensive design procedures for the inverter output filter in electric drives are described. In addition, these papers note that the deriving parasitic parameters on the conductive path have an important influence on the filter design and performance.

To achieve an overall optimal filter design, the accurate extraction of parasitic parameters and high-frequency models of CM impedance are key considerations. In [85], H. Chen *et al.* proposed a method for extracting the CM impedance of induction motors based on the measured values of CM voltage and current. An equivalent circuit of the CMV conductive loop was established, and the circuit parameters obtained by fitting the impedance curve to the measured values of CM voltage and current. Based on [85], nonlinear programming and a Monte Carlo algorithm were applied in [86] to fit the CM impedance curve of induction motors. The accuracy of the proposed extraction method was verified by comparing with the measured values of CM impedance.

B. ACTIVE EMI FILTERS

Active EMI filters, also referred to as active common noise canceller (ACC), is a CM voltage/current compensator used to reduce or even eliminate the CM EMI.

ACC first detects the CM voltage or current from the conductive path, then generates a reverse voltage or current using amplifier circuits, finally injects the reverse signals into the power circuit to realize the cancellation of CM interference. S. Ogasawara and H. Akagi first introduced ACC to motor drives in [87], [88].

A typical ACC, as depicted in Fig. 7, consists of a noise-sensing circuit, a noise-processing circuit, and a noise-compensating circuit [89]. In [87] and [88], three capacitors in parallel are used to detect the CMV of the inverter, then the amplifier circuit, fed from the DC bus, injects current into the primary side of the CM transformer, and hence inducing a compensation voltage opposing the CMV on the secondary side of the CM transformer, thereby cancelling the CMV. Experimental testing in [87] and [88] have verified that ACC can attenuate EMI in the 10KHz-3MHz band by 20dB.

The performance of ACC on CM EMI cancellation depends on the measurement accuracy of the CM signals. In [90] and [91], F. Blaabjerg *et al.* surveyed the commonly used methods for CM signals detection in ACC. M. Piazza improved the CM signal detection circuit, the amplifier circuit, and the CM transformer of ACC in [92], and used a dedicated DC power supply for the amplifier circuit,

TABLE 4. Summary of EMI filters key findings.

Method	Ref.	Cases	Theme	Frequency range of interest	Contribution
Passive EMI filters	[78-80]	Inverter fed induction motor	Designs passive filters to eliminate inverter-ground and motor frame-ground leakage currents	-	The RMS value of the leakage currents and the bearing current is reduced by more than 90%
	[81]	Inverter fed induction motor	Designs two filters inserted into both sides of the inverter to attenuate the CM EMI	150 kHz to 30 MHz	Greater than 40 dB reduction below 10 MHz and approximately 20 dB reduction at higher frequency (up to 30 MHz)
	[82]	Inverter fed AC motor	Compares the suppressing effects of inverter-end filter, motor-front-end filter and motor-chassis-end filter	Up to 10 MHz	Below 1 MHz, the filters show slight differences; From 1 MHz to 10 MHz, motor-front-end filter shows better performance
	[85][86]	Inverter fed induction motor	Extracts accurate CM impedance through equivalent CM circuit measuring CM voltage/current	Up to 10 MHz	Compared to two traditional methods, the estimated error of the proposed method is reduced by 10 dB
Active EMI filters	[87][88]	Inverter fed induction motor	Proposes the scheme of voltage-sensing voltage compensating active EMI filter	10 kHz to 3 MHz	Approximately 20 dBμV CMV reduction in low frequency (10 kHz to 3 MHz), but little or no reduction at higher frequency
	[92]	Inverter fed induction motor	Improves the detecting circuit, amplifier circuit and power supply of active filter to enhance the compensating ability	150 kHz to 30 MHz	About 10 dBμV CMV reduction in low frequency (below 1.5 MHz), but passive filter performs better at high frequency
	[93][94]	Three-level inverter fed induction motor	Directly connect the active filter to the AC side so that the CM transformer is cancelled	Integral multiples of switching frequency	Compared with passive filter, the 5^{th}, 11^{th}, and other higher harmonic currents are compensated
	[95]	Inverter fed induction motor	Integration of the active filter on the inverter drive circuit, thus eliminating CM transformer	10 kHz to 100 MHz	Average 15 dBμA reduction on CM current in 10 kHz to 0.5 MHz and average 5 dBμA reduction in 0.5 MHz to 10 MHz
	[96]	Inverter fed AC motor	Proposes a voltage-sensing current-compensating active filter which is based on a CM impedance network	150 kHz to 30 MHz	Average 10 dBμA reduction on DC side CM EMI below 3 MHz and average 5 dBμA reduction up to 30 MHz

improving the compensation performance of ACC. The CM transformer in ACC increases the cost and volume of ACC. By changing the injection location of the compensation voltage or current, the elimination of the CM transformer can be achieved. H. Akagi *et al.* designed a hybrid active filter which directly connects the ACC to the AC side through a passive RC filter in [93] and [94]. The passive filter has an additional function of power-factor correction for other inductive loads connected on the same 6.6-kV industrial power distribution system. Instead of compensating the voltage or current to the DC side or AC side, in [95], C. Zhu *et al.* injected compensations to the chassis relative to the inverter ground, so the CM transformer can be eliminated. In [96], Y. Zhang *et al.* build a CM impedance network on the AC side which has same CM impedance as the motor and injects the ACC compensation voltage into the AC side CM impedance network to generate a compensation current, with no transformer required. However, the effectiveness of the compensation for CM EMI depends on the matching of the AC-side impedance network and the load-side CM impedance. However, this match is difficult to achieve in practice because the motor on-load impedance is difficult to measure accurately.

An active filter is a compensation system that exhibits good CM EMI suppression in the low-frequency range. However, the performance of ACC is limited by many factors, such as the accurate measurement of system CM signals and impedance, and the reliability of the compensation circuit. Table 4 summarizes the reviewed papers on passive and active EMI filters.

IV. DISCUSSION

A. COMPARISON OF DIFFERENT SUPPRESSION METHODS

To better compare the attenuation band and amplitude provided by different methods, the spectral distribution of the maximum attenuation caused by different methods are presented in Fig. 8. Among each method, publications providing highest attenuation frequency and amplitude are included. The publications with an asterisk in Fig. 8 indicate that they have not been applied in motor drives. It should be noted that most of the EMI researches follow the measurement procedures and restrictions defined in corresponding EMI standards: IEC/CISPR ISM standards are followed by [24], [32], [81], [87] and others; DO 160 aeronautical standards are followed by [35], [73], [82]–[84] and others.

As can be seen from Fig. 8, research on the conductive EMI of motor and power converter is not limited to the range of 150 kHz-30 MHz. The main reason lies in:

a) The degree of electrical integration of equipment is increasing in many applications, such as EV/PHEV, robotics, etc. As a result of pursuing higher efficiency and power density, the layout of electrical system becomes more compact. Hence, the EMI at high frequency is more likely to interfere with other electronic components in the system. In addition, radiated EMI is mainly induced by the high-frequency

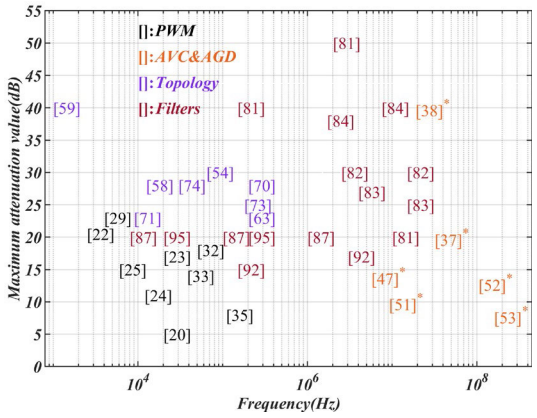

FIGURE 8. Spectral distribution of maximum attenuations of different methods.

circulating current flowing along the power cable. Therefore, EMI standards set limits on the EMI of electrical components over a wider range of frequencies. For example, CISPR25 [97] stipulates the limits and test configuration for conductive and radiated EMI in EV/PHEV from 150 kHz to 2500 MHz.

b) WBG device based electric drive has become a hotspot in academia and industry [98]–[100]. Although WBG devices have the potential to significantly improve the efficiency and power density of electric drives, the corner frequencies of the EMI spectrum are increased, incurring more severe EMI at high frequencies. A comparative study on conductive CM EMI of motor drives based on Si, SiC and GaN has been carried out in [101].

From the perspective of attenuation band, the attenuation bands of VSFPWM and complex topologies are below 30MHz, while the attenuation bands of AVC&AGD reach 300MHz. The reason for this phenomenon is that VSFPWM strategies suppress CM EMI by adjusting the duration d of voltage pulse, while AVC&AGD achieve it by improving the rise/fall transients t_r of voltage pulse. The duration of voltage pulse affects the first corner frequency in the EMI spectrum, while switching transients determine the higher corner frequency. Among VSFPWM strategies, the highest attenuation frequency occurs in [32], which employs model-predictive PWM. The highest attenuation frequency of complex topologies is provided by a dual-inverter fed dual-winding PMSM drive in [70]. In [53], an AGD adjusting R_g from 0.12Ω to 64 Ω achieves the highest attenuation frequency among the reviewed works.

From the perspective of attenuation amplitude, in the low-frequency range, complex topologies achieve higher attenuation than VSFPWM by eliminating ZCMV. The same effect can be achieved through ZCMV PWM in three-phase VSI [102], [103]. Generally, EMI attenuation at high frequency is smaller than that at low frequency, but 40dB attenuation at 20 MHz is achieved in [38] by shaping the transient voltage into an infinitely differentiable Gaussian transient.

In contrast to other methods achieving maximum attenuation in a narrow frequency band, passive filters can reflect EMI in a wider band through cascaded resonant circuits. It can be seen from Fig. 8 that cascaded filters can achieve maximum attenuation at multiple frequencies.

B. MERITS AND DRAWBACKS OF THE REVIEWED METHODS

VSFPWM does not require additional hardware, but it also has the lowest attenuation frequency and amplitude. Sole reliance on VSFPWM is likely to be sufficient in order to meet the EMI limits set in standards [35].

Compared with EMI filters, the attenuation bands realized with complex inverter topologies are narrower, while the cost of additional power devices and other associated circuitries is substantially higher. Therefore, suppressing EMI tends not to be the prime purpose of employing complex converter topologies. The adoption of complex topology is primarily concerned with features such as higher rating voltage, higher power, high reliability and other factors, such as the NPC three- level inverters adopted in medium-voltage high-power motor drives, with EMI dividends usually being something of a by-product.

Feedback based close-loop AVC&AGD are well suited to high switching frequency motor drives, although WBG devices, such as GaN FETs with faster switching transient and lower threshold voltage V_{th}, has yet to be widely adopted in motor drives. Although close-loop AVC&AGD show good EMI attenuation capability at high frequency, they have, to date, not been applied to motor drives. Nevertheless, an open-loop AGD based induction motor drive is reported in [104].

At the expense of increasing cost, volume, and weight, passive and active filters provide the highest attenuation and the widest attenuation band. They have been widely applied in different applications, such as EV/PHEV, aerospace sector, etc. However, the values of the passive components in filters are always somewhat over-designed to allow for EMI measurement accuracy and device ageing concerns.

C. COMPARISON ON HARDWARE COST AND CONTROL COMPLEXITY OF DIFFERENT METHODS

The decision on EMI suppression scheme always has cost constraints, both on hardware cost and control complexity. To provide a general concept on the cost of each method, the hardware cost and control complexity of the reviewed methods are compared in Fig. 9. The costs of filters have not been discussed in Fig. 9. The reason lies in:

a) The methods suppressing EMI from sources have generality, indicating that the costs of these methods are independent of system requirements on rated voltage, power, power density, reliability, lifetime, etc.

b) The costs of passive/active filters are highly dependent on the system requirements mentioned above. Hence, the costs of filters can hardly be compared with the costs

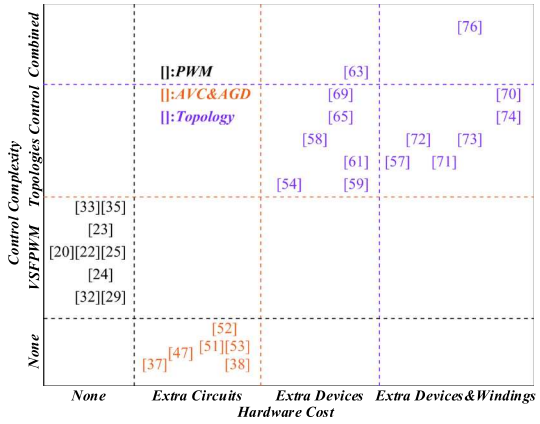

FIGURE 9. Comparison on hardware cost and control complexity of different methods mitigating EMI from sources.

of the other methods in the same scope and will be studied independently.

As indicated in the Fig. 9, the VSFPWM and AVC&AGD do not contribute to extra hardware costs and control complexity, respectively. Among the VSFPWM methods, the model predictive VSFPWM [33], [35] has the highest control complexity due to the current ripple prediction and the switching period calculation process, whereas the periodic RPWM [29], [32] has the lowest control complexity owing to the easy implementation of periodic waveforms in digital controllers. Among AVC&AGD methods, the programmable driving IC in [53] and the voltage control circuits in [38] bring the highest extra hardware cost. Compared with the non-programmable ASIC IC in [52], the programmable IC in [53] has the extra clock, memory, op-amp circuits. In [38], the extra cost is introduced by the *RC* resonant circuit used as the feedback path and the op circuits used to regulate the V_{CE}.

The extra power devices and their driving circuits posed by complex topologies introduce more cost both on hardware and control complexity. The four-leg inverter in [54] requires 8 power devices and an *LC* filter. Furthermore, the 3-level four-leg inverter in [57] requires 24 power devices and an *LC* filter, which makes its hardware cost far more than the traditional four-leg inverter [57] and 3-level inverters composed of 12 power switches and 6 diodes [59], [61], [63]. The paralleled inverters [65], [69] have the same amount of power switches as the 3-level inverters have, but the coupling inductors also contribute to the hardware cost of paralleled inverters. From the perspective of control complexity, the ZCMV PWM for 3-level inverters are combined with VSFPWM in [63], resulting in highest control complexity, and the simplest control occurs at [54], [59] since they only adopt the ZCMV PWM for the traditional four-leg inverter and 3-level inverter.

Although the coupling inductors in paralleled inverters are cancelled in paralleled inverter fed dual-three phase motors, the winding configurations and the special manufacturing process of dual three-phase or dual-segment motors propose more hardware cost. In [72], the paralleled inverter is simplified as two 4-switches inverters to drive the dual three-phase motor, hence reducing 4 power devices compared to [71]. Besides, the two-segment motors [70], [74] introduce more hardware cost than the conventional dual three-phase motors [73], [76] due to their special manufacturing process. The control strategy adopted in [71], [72] is the same as a conventional inverter [71], while phase-shifting PWM is employed in [70], [73], [74] to achieve ZCMV control. The model predictive VSFPWM for the dual three-phase motor in [76] brings the highest control complexity.

TABLE 5. Costs of passive and active filters.

REF.	CM Passive Components	Active Components
[78]	*L*: 9 mH, 28 mH; *C*: 0.047 μF * 3; *R*: 100 Ω.	-
[79]	*L*: 10 mH *2; *C*: 0.22 μF *2; *R*: 50 Ω *2.	-
[80]	*L*: 76 mH; *C*: 100 nF *2; *R*: 100 Ω.	-
[81]	*L*: 100 μH, 54 μH, 18 mH; *C*: 1 μF *3, 0.22 μF.	-
[84]	*C*: 50 nF*3; CM Choke: 200μH *2.	-
[87]	*C*: 180 pF *3, 1 μF *2; CM Transformer.	A push-pull emitter follower.
[92]	*C*: 0.5 nF *3, 6 nF, 47 μF *2; CM Transformer.	A Darlington push-pull circuit; A converter.
[95]	*C*: 1 nF *3.	A buffer op-amp circuit; An inverting circuit.
[96]	*C*: 2.2 μF; *R*: 5.1-3k Ω *8.	2 op-amp circuits; 1 push-pull circuit; 2 diodes.

The comparison of passive and active components of filters is presented in Table 5. The inductance components are necessary for passive filters, and the values of passive components are dependent on the filter configurations. However, the usage of passive components has a reduction in active filters, especially in transformerless active filters [95], [96], in which the filters are integrated in motor drives. The power density of active filters is significantly increased due to the reduction of passive components, but the op-amp circuits with wide unity-gain bandwidth are required.

D. DISCUSSION ON FUTURE DEVELOPMENT OF EMI SUPPRESSION METHOD

Although various EMI suppression methods have been proposed, EMI filters remain an essential component in motor drives. In the design and implementation of passive/active filters, EMI measurement and sensing play critical roles.

In the design of passive filters, the conductive EMI is measured experimentally using equipment such as LISN, radiated frequency probe, spectrum analyzer, etc. The structure and values of passive components are determined by the measurement results. However, the inductances and capacitances in filters are prone to ageing under the influence of temperature [105], [106], thus reducing the performance and efficiency of the filters over time. Furthermore, the ageing of the motor and its drive also result in some shifts in the

EMI spectrum, which exacerbates the deterioration of EMI filters.

In active EMI filters, conductive EMI is sensed by resonant circuits, and various sensing circuits are summarized in [89]. The compensating effect of active filters is limited by the sensing precision of the resonant frequencies. Furthermore, the effectiveness of traditional active EMI filter for volume reduction is limited due to the use of passive components in the sensing circuit [107].

In order to further reduce the cost, volume, and weight of EMI filters, and improve their attenuating ability and efficiency, real-time EMI monitoring with low hardware cost could play a key role in the future development. EMI real-time monitoring aims to sense and predict conductive EMI based on accurate predictive model and system feedbacks. Several advancements could be achieved based on EMI real-time monitoring.

a) Life cycle dynamic passive filter. Based on EMI real-time monitoring, the parameters and even configuration of passive filters can be dynamically adjusted through low-cost switching circuits to deal with EMI deterioration caused by component ageing.

b) The active filter without EMI sensing circuit. EMI real-time monitoring can be used to replace the EMI sensing circuit composed of passive components, which can further reduce the volume and weight of active EMI filters.

V. CONCLUSION

In this paper, representative methods of suppressing conductive EMI in motor drives have been reviewed from several perspectives. The methods are divided into two categories, viz. mitigation of EMI from the source and suppression EMI on its propagation path. Furthermore, the characteristic of each method is discussed and the mechanisms are illustrated. The application cases, the effective frequency range, and the suppression level are summarized. Finally, the attenuation band and attenuation level of each method are compared, and the future development opportunities for EMI suppression methods are discussed.

REFERENCES

[1] *Environmental Conditions and Test Procedures for Airborne Equipment*, document DO-160G, 2010.

[2] *Industrial, Scientific and Medical Equipment–Radio-Frequency Disturbance Characteristics–Limits and Methods of Measurement*, document CISPR 11, 2015.

[3] *Electromagnetic Compatibility of Multimedia Equipment–Emission Requirements*, document CISPR 32, 2015.

[4] *Requirements For The Control Of Electromagnetic Interference Characteristics Of Subsystems And Equipment*, document MIL-STD-461G, 2015.

[5] A. Muetze and A. Binder, "Calculation of motor capacitances for prediction of the voltage across the bearings in machines of inverter-based drive systems," *IEEE Trans. Ind. Appl.*, vol. 43, no. 3, pp. 665–672, May 2007, doi: 10.1109/TIA.2007.895734.

[6] R. Naik, T. A. Nondahl, M. J. Melfi, R. Schiferl, and J.-S. Wang, "Circuit model for shaft voltage prediction in induction motors fed by PWM-based AC drives," *IEEE Trans. Ind. Appl.*, vol. 39, no. 5, pp. 1294–1299, Sep. 2003, doi: 10.1109/TIA.2003.816504.

[7] D. Busse, J. Erdman, R. J. Kerkman, D. Schlegel, and G. Skibinski, "System electrical parameters and their effects on bearing currents," *IEEE Trans. Ind. Appl.*, vol. 33, no. 2, pp. 577–584, Mar. 1997, doi: 10.1109/28.568025.

[8] A. F. Moreira, T. A. Lipo, G. Venkataramanan, and S. Bernet, "High-frequency modeling for cable and induction motor overvoltage studies in long cable drives," *IEEE Trans. Ind. Appl.*, vol. 38, no. 5, pp. 1297–1306, Sep. 2002, doi: 10.1109/TIA.2002.802920.

[9] C. Marlier, A. Videt, and N. Idir, "NIF-based frequency-domain modeling method of three-wire shielded energy cables for EMC simulation," *IEEE Trans. Electromagn. Compat.*, vol. 57, no. 1, pp. 145–155, Feb. 2015, doi: 10.1109/TEMC.2014.2359514.

[10] A. Cataliotti, D. D. Cara, G. Marsala, A. Pecoraro, A. Ragusa, and G. Tine, "High-frequency experimental characterization and modeling of six pack IGBTs power modules," *IEEE Trans. Ind. Electron.*, vol. 63, no. 11, pp. 6664–6673, Nov. 2016, doi: 10.1109/TIE.2016.2585082.

[11] A. Nejadpak and O. A. Mohammed, "Physics-based modeling of power converters from finite element electromagnetic field computations," *IEEE Trans. Magn.*, vol. 49, no. 1, pp. 567–576, Jan. 2013, doi: 10.1109/TMAG.2012.2206046.

[12] H. Zhang and A. Wu, "Common-mode noise reduction by parasitic capacitance cancellation in the three-phase inverter," *IEEE Trans. Electromagn. Compat.*, vol. 61, no. 1, pp. 295–300, Feb. 2019, doi: 10.1109/TEMC.2017.2787780.

[13] A. D. Brovont and A. N. Lemmon, "Utilization of power module baseplate capacitance for common-mode EMI filter reduction," in *Proc. IEEE Electric Ship Technol. Symp. (ESTS)*, Aug. 2019, pp. 403–408, doi: 10.1109/ESTS.2019.8847829.

[14] X. Gong and J. A. Ferreira, "Investigation of conducted EMI in SiC JFET inverters using separated heat sinks," *IEEE Trans. Ind. Electron.*, vol. 61, no. 1, pp. 115–125, Jan. 2014, doi: 10.1109/TIE.2013.2240636.

[15] Z. Fang, D. Jiang, Z. Shen, and R. Qu, "Impact of application of SiC devices in motor drive on EMI," in *Proc. IEEE Appl. Power Electron. Conf. Expo. (APEC)*, Mar. 2017, pp. 652–658, doi: 10.1109/APEC.2017.7930763.

[16] L. Yang, S. Wang, and J. Feng, "Advances in electromagnetic interference modeling and noise reduction for adjustable speed motor drive systems," in *Proc. IEEE Int. Symp. Electromagn. Compat. Signal/Power Integrity (EMCSI)*, Aug. 2017, pp. 249–254, doi: 10.1109/ISEMC.2017.8077875.

[17] B. Zhang and S. Wang, "A survey of EMI research in power electronics systems with wide-bandgap semiconductor devices," *IEEE J. Emerg. Sel. Topics Power Electron.*, vol. 8, no. 1, pp. 626–643, Mar. 2020, doi: 10.1109/JESTPE.2019.2953730.

[18] A. Amin and S. Choi, "A review on recent characterization effort of CM EMI in power electronics system with emerging wide band gap switch," in *Proc. IEEE Electric Ship Technol. Symp. (ESTS)*, Aug. 2019, pp. 241–248, doi: 10.1109/ESTS.2019.8847800.

[19] S. Natarajan, T. Sudhakar Babu, K. Balasubramanian, U. Subramaniam, and D. J. Almakhles, "A state-of-the-art review on conducted electromagnetic interference in non-isolated DC to DC converters," *IEEE Access*, vol. 8, pp. 2564–2577, 2020, doi: 10.1109/ACCESS.2019.2961954.

[20] T. Pu, F. Bu, W. Huang, and L. Zhu, "Implementation of random SVPWM strategy for three-phase voltage source inverter based on FPGA," in *Proc. 20th Int. Conf. Electr. Mach. Syst. (ICEMS)*, Aug. 2017, pp. 8–11, doi: 10.1109/ICEMS.2017.8056142.

[21] T. S. Sivarani, S. J. Jawhar, and C. A. Kumar, "Intensive random carrier pulse width modulation for induction motor drives based on hopping between discrete carrier frequencies," *IET Power Electron.*, vol. 9, no. 3, pp. 417–426, Mar. 2016, doi: 10.1049/iet-pel.2015.0477.

[22] Y. Zhang, Z. Yin, J. Liu, R. Zhang, and X. Sun, "IPMSM sensorless control using high-frequency voltage injection method with random switching frequency for audible noise improvement," *IEEE Trans. Ind. Electron.*, vol. 67, no. 7, pp. 6019–6030, Jul. 2020, doi: 10.1109/TIE.2019.2937042.

[23] K. Lee, G. Shen, W. Yao, and Z. Lu, "Performance characterization of random pulse width modulation algorithms in industrial and commercial adjustable-speed drives," *IEEE Trans. Ind. Appl.*, vol. 53, no. 2, pp. 1078–1087, Mar. 2017, doi: 10.1109/TIA.2016.2616407.

[24] P. Lezynski, "Random modulation in inverters with respect to electromagnetic compatibility and power quality," *IEEE J. Emerg. Sel. Topics Power Electron.*, vol. 6, no. 2, pp. 782–790, Jun. 2018, doi: 10.1109/JESTPE.2017.2787599.

[25] A. C. B. Kumar and G. Narayanan, "Variable-switching frequency PWM technique for induction motor drive to spread acoustic noise spectrum with reduced current ripple," *IEEE Trans. Ind. Appl.*, vol. 52, no. 5, pp. 3927–3938, Sep. 2016, doi: 10.1109/TIA.2016.2561259.

[26] A. Santolaria, J. Balcells, and D. Gonzalez, "Theoretical and experimental results of power converter frequency modulation," in *Proc. IEEE 28th Annu. Conf. Ind. Electron. Soc. (IECON)*, vol. 1, Nov. 2002, pp. 193–197, doi: 10.1109/IECON.2002.1187505.

[27] A. Santolaria, J. Balcells, D. Gonzalez, and J. Gago, "Evaluation of switching frequency modulation in EMI emissions reduction applied to power converters," in *Proc. 29th Annu. Conf. IEEE Ind. Electron. Soc. (IECON)*, vol. 3, 2003, pp. 5–10, doi: 10.1109/IECON.2003.1280604.

[28] J. Balcells, A. Santolaria, A. Orlandi, D. Gonzalez, and J. Gago, "EMI reduction in switched power converters using frequency modulation techniques," *IEEE Trans. Electromagn. Compat.*, vol. 47, no. 3, pp. 569–576, Aug. 2005, doi: 10.1109/TEMC.2005.851733.

[29] X. Yongxiang, Y. Qingbing, Z. Jibin, and W. Hao, "Influence of periodic carrier frequency modulation on inverter loss of permanent magnet synchronous motor drive system," in *Proc. 17th Int. Conf. Electr. Mach. Syst. (ICEMS)*, Oct. 2014, pp. 2101–2106, doi: 10.1109/ICEMS.2014.7013832.

[30] D. Gonzalez, J. Balcells, A. Santolaria, J.-C. Le Bunetel, J. Gago, D. Magnon, and S. Brehaut, "Conducted EMI reduction in power converters by means of periodic switching frequency modulation," *IEEE Trans. Power Electron.*, vol. 22, no. 6, pp. 2271–2281, Nov. 2007, doi: 10.1109/TPEL.2007.909257.

[31] X. Yongxiang, Y. Qingbing, Z. Jibin, and W. Hao, "Influence of periodic carrier frequency modulation on stator steel core loss and rotor eddy current loss of permanent magnet synchronous motor," in *Proc. 17th Int. Conf. Electr. Mach. Syst. (ICEMS)*, Oct. 2014, pp. 2094–2100, doi: 10.1109/ICEMS.2014.7013850.

[32] X. Yongxiang, Y. Qingbing, Z. Jibin, W. Baochao, and L. Junlong, "Periodic carrier frequency modulation in reducing low-frequency electromagnetic interference of permanent magnet synchronous motor drive system," *IEEE Trans. Magn.*, vol. 51, no. 11, pp. 1–4, Nov. 2015, doi: 10.1109/TMAG.2015.2440293.

[33] D. Jiang and F. Wang, "Variable switching frequency PWM for three-phase converters based on current ripple prediction," *IEEE Trans. Power Electron.*, vol. 28, no. 11, pp. 4951–4961, Nov. 2013, doi: 10.1109/TPEL.2013.2240701.

[34] D. Jiang and F. Wang, "Current-ripple prediction for three-phase PWM converters," *IEEE Trans. Ind. Appl.*, vol. 50, no. 1, pp. 531–538, Jan. 2014, doi: 10.1109/TIA.2013.2270224.

[35] D. Jiang, Q. Li, and Z. Shen, "Model predictive PWM for AC motor drives," *IET Electr. Power Appl.*, vol. 11, no. 5, pp. 815–822, May 2017, doi: 10.1049/iet-epa.2016.0456.

[36] N. Oswald, B. H. Stark, D. Holliday, C. Hargis, and B. Drury, "Analysis of shaped pulse transitions in power electronic switching waveforms for reduced EMI generation," *IEEE Trans. Ind. Appl.*, vol. 47, no. 5, pp. 2154–2165, Sep. 2011, doi: 10.1109/TIA.2011.2161971.

[37] N. Oswald, P. Anthony, N. McNeill, and B. H. Stark, "An experimental investigation of the tradeoff between switching losses and EMI generation with hard-switched all-Si, Si-siC, and all-siC device combinations," *IEEE Trans. Power Electron.*, vol. 29, no. 5, pp. 2393–2407, May 2014, doi: 10.1109/TPEL.2013.2278919.

[38] X. Yang, Y. Yuan, X. Zhang, and P. R. Palmer, "Shaping high-power IGBT switching transitions by active voltage control for reduced EMI generation," *IEEE Trans. Ind. Appl.*, vol. 51, no. 2, pp. 1669–1677, Mar. 2015, doi: 10.1109/TIA.2014.2347578.

[39] X. Yang, Z. Long, Y. Wen, H. Huang, and P. R. Palmer, "Investigation of the trade-off between switching losses and EMI generation in Gaussian S-shaping for high-power IGBT switching transients by active voltage control," *IET Power Electron.*, vol. 9, no. 9, pp. 1979–1984, Jul. 2016, doi: 10.1049/iet-pel.2015.1035.

[40] X. Yang, M. Otsuki, and P. R. Palmer, "Physics-based insulated-gate bipolar transistor model with input capacitance correction," *IET Power Electron.*, vol. 8, no. 3, pp. 417–427, Mar. 2015, doi: 10.1049/iet-pel.2014.0169.

[41] N. Idir, R. Bausiere, and J. J. Franchaud, "Active gate voltage control of turn-on di/dt and turn-off dv/dt in insulated gate transistors," *IEEE Trans. Power Electron.*, vol. 21, no. 4, pp. 849–855, Jul. 2006, doi: 10.1109/TPEL.2007.876895.

[42] Y. S. Cheng, T. Mannen, K. Wada, K. Miyazaki, M. Takamiya, and T. Sakurai, "Optimization platform to find a switching pattern of digital active gate drive for reducing both switching loss and surge voltage," *IEEE Trans. Ind. Appl.*, vol. 55, no. 5, pp. 5023–5031, Sep. 2019, doi: 10.1109/TIA.2019.2927462.

[43] R. Wang, L. Liang, Y. Chen, Y. Pan, J. Li, L. Han, and G. Tan, "Self-adaptive active gate driver for IGBT switching performance optimization based on status monitoring," *IEEE Trans. Power Electron.*, vol. 35, no. 6, pp. 6362–6372, Jun. 2020, doi: 10.1109/TPEL.2019.2947268.

[44] Z. Zhang, Z. Wang, F. Wang, L. M. Tolbert, and B. J. Blalock, "Reliability-oriented design of gate driver for SiC devices in voltage source converter," in *Proc. IEEE Int. Workshop Integr. Power Packag. (IWIPP)*, May 2015, pp. 20–23, doi: 10.1109/IWIPP.2015.7295968.

[45] A. Choudhury, "Present status of SiC based power converters and gate drivers—A review," in *Proc. Int. Power Electron. Conf. IPEC-Niigata-ECCE Asia*, 2018, pp. 3401–3405, doi: 10.23919/IPEC.2018.8507554.

[46] Y. Liu and Y. Yang, "Review of SiC MOSFET drive circuit," in *Proc. IEEE Int. Conf. Electron Devices Solid-State Circuits (EDSSC)*, Jun. 2019, pp. 1–3, doi: 10.1109/EDSSC.2019.8754378.

[47] A. Paredes, V. Sala, H. Ghorbani, and L. Romeral, "A novel active gate driver for silicon carbide MOSFET," in *Proc. 42nd Annu. Conf. IEEE Ind. Electron. Soc. (IECON)*, Oct. 2016, pp. 3172–3177, doi: 10.1109/IECON.2016.7793222.

[48] A. P. Camacho, V. Sala, H. Ghorbani, and J. L. R. Martinez, "A novel active gate driver for improving SiC MOSFET switching trajectory," *IEEE Trans. Ind. Electron.*, vol. 64, no. 11, pp. 9032–9042, Nov. 2017, doi: 10.1109/TIE.2017.2719603.

[49] P. Nayak and K. Hatua, "Active gate driving technique for a 1200 v SiC MOSFET to minimize detrimental effects of parasitic inductance in the converter layout," in *Proc. IEEE Energy Convers. Congr. Exposit. (ECCE)*, Sep. 2016, pp. 1–8, doi: 10.1109/ECCE.2016.7854819.

[50] P. Nayak and K. Hatua, "Active gate driving technique for a 1200 v SiC MOSFET to minimize detrimental effects of parasitic inductance in the converter layout," *IEEE Trans. Ind. Appl.*, vol. 54, no. 2, pp. 1622–1633, Mar. 2018, doi: 10.1109/TIA.2017.2780175.

[51] Y. Yang, Y. Wen, and Y. Gao, "A novel active gate driver for improving switching performance of high-power SiC MOSFET modules," *IEEE Trans. Power Electron.*, vol. 34, no. 8, pp. 7775–7787, Aug. 2019, doi: 10.1109/TPEL.2018.2878779.

[52] P. Bau, M. Cousineau, B. Cougo, F. Richardeau, and N. Rouger, "CMOS active gate driver for closed-loop dv/dt control of GaN transistors," *IEEE Trans. Power Electron.*, vol. 35, no. 12, pp. 13322–13332, Dec. 2020, doi: 10.1109/TPEL.2020.2995531.

[53] H. C. P. Dymond, J. Wang, D. Liu, J. J. O. Dalton, N. McNeill, D. Pamunuwa, S. J. Hollis, and B. H. Stark, "A 6.7-GHz active gate driver for GaN FETs to combat overshoot, ringing, and EMI," *IEEE Trans. Power Electron.*, vol. 33, no. 1, pp. 581–594, Jan. 2018, doi: 10.1109/TPEL.2017.2669879.

[54] A. L. Julian, G. Oriti, and T. A. Lipo, "Elimination of common-mode voltage in three-phase sinusoidal power converters," *IEEE Trans. Power Electron.*, vol. 14, no. 5, pp. 982–989, Sep. 1999, doi: 10.1109/63.788504.

[55] R. Zhang, D. Boroyevich, V. H. Prasad, H.-C. Mao, F. C. Lee, and S. Dubovsky, "A three-phase inverter with a neutral leg with space vector modulation," in *Proc. Appl. Power Electron. Conf. (APEC)*, vol. 2, no. 1, 1997, pp. 857–863, doi: 10.1109/apec.1997.575746.

[56] R. Zhang, V. H. Prasad, D. Boroyevich, and F. C. Lee, "Three-dimensional space vector modulation for four-leg voltage-source converters," *IEEE Trans. Power Electron.*, vol. 17, no. 3, pp. 314–326, May 2002.

[57] R. Chen, J. Niu, H. Gui, Z. Zhang, F. Wang, L. M. Tolbert, B. J. Blalock, D. J. Costinett, and B. B. Choi, "Investigation of fourth-leg for common-mode noise reduction in three-level neutral point clamped inverter fed motor drive," in *Proc. IEEE Appl. Power Electron. Conf. Expo. (APEC)*, Mar. 2019, pp. 2582–2588, doi: 10.1109/APEC.2019.8722319.

[58] P. Garg, S. Essakiappan, H. S. Krishnamoorthy, and P. N. Enjeti, "A fault-tolerant three-phase adjustable speed drive topology with active common-mode voltage suppression," *IEEE Trans. Power Electron.*, vol. 30, no. 5, pp. 2828–2839, May 2015, doi: 10.1109/TPEL.2014.2361905.

[59] F. Wang, A. K. Wallace, S. Dai, A. Von Jouanne, and H. Zhang, "Multi-level inverter modulation schemes to eliminate common-mode voltages," *IEEE Trans. Ind. Appl.*, vol. 36, no. 6, pp. 1645–1653, Nov. 2000, doi: 10.1109/28.887217.

[60] M. Duang-upra and Y. Kamsuwan, "Three-segment switching sequences for a space-vector modulated three-level inverter to eliminate common-mode voltages," in *Proc. 45th Annu. Conf. IEEE Ind. Electron. Soc. (IECON)*, Oct. 2019, pp. 2082–2087, doi: 10.1109/IECON.2019.8927324.

[61] T.-K.-T. Nguyen, N.-V. Nguyen, and N. R. Prasad, "Novel eliminated common-mode voltage PWM sequences and an online algorithm to reduce current ripple for a three-level inverter," *IEEE Trans. Power Electron.*, vol. 32, no. 10, pp. 7482–7493, Oct. 2017, doi: 10.1109/TPEL.2016.2634009.

[62] L. Kai, J. Zhao, W. Wu, M. Li, L. Ma, and G. Zhang, "Performance analysis of zero common-mode voltage pulse-width modulation techniques for three-level neutral point clamped inverters," *IET Power Electron.*, vol. 9, no. 14, pp. 2654–2664, Nov. 2016, doi: 10.1049/iet-pel.2016.0009.

[63] J. Chen, D. Jiang, W. Sun, Z. Shen, and Y. Zhang, "An improved variable switching frequency modulation strategy for three-level converters with reduced conducted EMI," in *Proc. IEEE Energy Convers. Congr. Expo. (ECCE)*, Sep. 2019, pp. 6937–6942, doi: 10.1109/ECCE.2019.8913252.

[64] X. Xing, A. Chen, Z. Zhang, J. Chen, and C. Zhang, "Model predictive control method to reduce common-mode voltage and balance the neutral-point voltage in three-level T-type inverter," in *Proc. IEEE Appl. Power Electron. Conf. Expo. (APEC)*, Mar. 2016, pp. 3453–3458, doi: 10.1109/APEC.2016.7468363.

[65] D. Zhang, F. Wang, R. Burgos, R. Lai, and D. Boroyevich, "Impact of interleaving on AC passive components of paralleled three-phase voltage-source converters," *IEEE Trans. Ind. Appl.*, vol. 46, no. 3, pp. 1042–1054, Mar. 2010, doi: 10.1109/TIA.2010.2045336.

[66] D. Zhang, F. Wang, R. Burgos, and D. Boroyevich, "Total flux minimization control for integrated inter-phase inductors in paralleled, interleaved three-phase two-level voltage-source converters with discontinuous space-vector modulation," *IEEE Trans. Power Electron.*, vol. 27, no. 4, pp. 1679–1688, Apr. 2012, doi: 10.1109/TPEL.2011.2169281.

[67] D. Zhang, F. Wang, R. Burgos, and D. Boroyevich, "Common-mode circulating current control of paralleled interleaved three-phase two-level voltage-source converters with discontinuous space-vector modulation," *IEEE Trans. Power Electron.*, vol. 26, no. 12, pp. 3925–3935, Dec. 2011, doi: 10.1109/TPEL.2011.2131681.

[68] D. Jiang and Z. Shen, "Paralleled inverters with zero common-mode voltage," in *Proc. IEEE Energy Convers. Congr. Expo. (ECCE)*, Sep. 2016, pp. 1–8, doi: 10.1109/ECCE.2016.7855330.

[69] D. Jiang, Z. Shen, and F. Wang, "Common-mode voltage reduction for paralleled inverters," *IEEE Trans. Power Electron.*, vol. 33, no. 5, pp. 3961–3974, May 2018, doi: 10.1109/TPEL.2017.2712369.

[70] Z. Shen, D. Jiang, T. Zou, and R. Qu, "Dual-segment three-phase PMSM with dual inverters for leakage current and common-mode EMI reduction," *IEEE Trans. Power Electron.*, vol. 34, no. 6, pp. 5606–5619, Jun. 2019, doi: 10.1109/TPEL.2018.2866338.

[71] A. von Jauanne and H. Zhang, "A dual-bridge inverter approach to eliminating common-mode voltages and bearing and leakage currents," *IEEE Trans. Power Electron.*, vol. 14, no. 1, pp. 43–48, Jan. 1999, doi: 10.1109/63.737591.

[72] H. Zhang, A. Von Jouanne, and S. Dai, "A reduced-switch dual-bridge inverter topology for the mitigation of bearing currents, EMI, and DC-link voltage variations," *IEEE Trans. Ind. Appl.*, vol. 37, no. 5, pp. 1365–1372, 2001, doi: 10.1109/28.952512.

[73] Z. Shen, D. Jiang, Z. Liu, D. Ye, and J. Li, "Common-mode voltage elimination for dual two-level inverter-fed asymmetrical six-phase PMSM," *IEEE Trans. Power Electron.*, vol. 35, no. 4, pp. 3828–3840, Apr. 2020, doi: 10.1109/TPEL.2019.2933446.

[74] X. Han, D. Jiang, T. Zou, R. Qu, and K. Yang, "Two-segment three-phase PMSM drive with carrier phase-shift PWM for torque ripple and vibration reduction," *IEEE Trans. Power Electron.*, vol. 34, no. 1, pp. 588–599, Jan. 2019, doi: 10.1109/TPEL.2018.2824808.

[75] X. Han, D. Jiang, T. Zou, R. Qu, and K. Yang, "Two-segment three-phase PMSM drive with carrier phase-shift PWM," in *Proc. IEEE Appl. Power Electron. Conf. Expo. (APEC)*, Mar. 2018, pp. 848–854, doi: 10.1109/APEC.2018.8341112.

[76] D. Ye, J. Li, R. Qu, D. Jiang, L. Xiao, Y. Lu, and J. Chen, "Variable switching sequence PWM strategy of dual three-phase machine drive for high-frequency current harmonic suppression," *IEEE Trans. Power Electron.*, vol. 35, no. 5, pp. 4984–4995, May 2020, doi: 10.1109/TPEL.2019.2941991.

[77] C. Jettanasen, "Analysis of conducted electromagnetic interference generated by PWM inverter fed-AC motor drives," in *Proc. 15th Int. Conf. Electr. Mach. Syst. (ICEMS)*, 2012, pp. 1–6.

[78] H. Akagi and T. Doumoto, "A passive EMI filter for preventing high-frequency leakage current from flowing through the grounded inverter heat sink of an adjustable-speed motor drive system," *IEEE Trans. Ind. Appl.*, vol. 41, no. 5, pp. 1215–1223, Sep. 2005, doi: 10.1109/TIA.2005.853391.

[79] H. Akagi and T. Oe, "A specific filter for eliminating high-frequency leakage current from the grounded heat sink in a motor drive with an active front end," *IEEE Trans. Power Electron.*, vol. 23, no. 2, pp. 763–770, Mar. 2008, doi: 10.1109/TPEL.2007.915673.

[80] H. Akagi and S. Tamura, "A passive EMI filter for eliminating both bearing current and ground leakage current from an inverter-driven motor," *IEEE Trans. Power Electron.*, vol. 21, no. 5, pp. 1459–1469, Sep. 2006, doi: 10.1109/TPEL.2006.880239.

[81] H. Akagi and T. Shimizu, "Attenuation of conducted EMI emissions from an inverter-driven motor," *IEEE Trans. Power Electron.*, vol. 23, no. 1, pp. 282–290, Jan. 2008, doi: 10.1109/TPEL.2007.911878.

[82] J. Xue, F. Wang, and W. Chen, "A study of motor-end EMI filter on output common-mode noise suppression in DC-fed motor drive system," in *Proc. 28th Annu. IEEE Appl. Power Electron. Conf. Expo. (APEC)*, Mar. 2013, pp. 1556–1561, doi: 10.1109/APEC.2013.6520504.

[83] J. Xue, F. Wang, X. Zhang, D. Boroyevich, and P. Mattavelli, "Design of output passive EMI filter in DC-fed motor drive," in *Proc. 27thAnnu. IEEE Appl. Power Electron. Conf. Expo. (APEC)*, Feb. 2012, pp. 634–640, doi: 10.1109/APEC.2012.6165885.

[84] J. Xue, F. Wang, and B. Guo, "EMI noise mode transformation due to propagation path unbalance in three-phase motor drive system and its implication to EMI filter design," in *Proc. IEEE Appl. Power Electron. Conf. Expo. (APEC)*, Mar. 2014, pp. 806–811, doi: 10.1109/APEC.2014.6803400.

[85] H. Chen, Y. Yan, and H. Zhao, "Extraction of common-mode impedance of an inverter-fed induction motor," *IEEE Trans. Electromagn. Compat.*, vol. 58, no. 2, pp. 599–606, Apr. 2016, doi: 10.1109/TEMC.2016.2519543.

[86] H. Chen and S. Ye, "Modeling of common-mode impedance of an inverter-fed induction motor from online measurement," *IEEE Trans. Electromagn. Compat.*, vol. 60, no. 5, pp. 1581–1589, Oct. 2018, doi: 10.1109/TEMC.2017.2779886.

[87] S. Ogasawara, H. Ayano, and H. Akagi, "An active circuit for cancellation of common-mode voltage generated by a PWM inverter," *IEEE Trans. Power Electron.*, vol. 13, no. 5, pp. 835–841, Sep. 1998, doi: 10.1109/63.712285.

[88] S. Ogasawara, H. Ayano, and H. Akagi, "An active circuit for cancellation of common-mode voltage generated by a PWM inverter," in *Proc. Rec. 28th Annu. IEEE Power Electron. Spec. Conf. Formerly Power Conditioning Spec. Conf. 71st Power Process. Electron. Spec. Conf. (PESC)*, vol. 2, 1997, pp. 1547–1553, doi: 10.1109/PESC.1997.618067.

[89] B. Narayanasamy and F. Luo, "A survey of active EMI filters for conducted EMI noise reduction in power electronic converters," *IEEE Trans. Electromagn. Compat.*, vol. 61, no. 6, pp. 2040–2049, Dec. 2019, doi: 10.1109/TEMC.2019.2953055.

[90] L. Asiminoael, F. Blaabjerg, and S. Hansen, "Detection is key–harmonic detection methods for active power filter applications," *IEEE Ind. Appl. Mag.*, vol. 13, no. 4, pp. 22–33, Jul. 2007, doi: 10.1109/MIA.2007.4283506.

[91] K. Sergej, L. Asiminoaei, and S. Hansen, "Harmonic detection methods of active filters for adjustable speed drive applications," in *Proc. 13th Eur. Conf. Power Electron. Appl. (EPE)*, vol. 9, 2009, pp. 1–10.

[92] M. C. Di Piazza, G. Tine, and G. Vitale, "An improved active common-mode voltage compensation device for induction motor drives," *IEEE Trans. Ind. Electron.*, vol. 55, no. 4, pp. 1823–1834, Apr. 2008, doi: 10.1109/TIE.2008.917063.

[93] H. Akagi and T. Hatada, "Voltage balancing control for a three-level diode-clamped converter in a medium-voltage transformerless hybrid active filter," *IEEE Trans. Power Electron.*, vol. 24, no. 3, pp. 571–579, Mar. 2009, doi: 10.1109/TPEL.2009.2012528.

[94] H. Akagi and R. Kondo, "A transformerless hybrid active filter using a three-level pulsewidth modulation (PWM) converter for a medium-voltage motor drive," *IEEE Trans. Power Electron.*, vol. 25, no. 6, pp. 1365–1374, Jun. 2010, doi: 10.1109/TPEL.2009.2040002.

[95] C. Zhu and T. H. Hubing, "An active cancellation circuit for reducing electrical noise from three-phase AC motor drivers," *IEEE Trans. Electromagn. Compat.*, vol. 56, no. 1, pp. 60–66, Feb. 2014, doi: 10.1109/TEMC.2013.2267801.
[96] Y. Zhang, Q. Li, and D. Jiang, "A motor CM impedance based transformerless active EMI filter for DC-side common-mode EMI suppression in motor drive system," *IEEE Trans. Power Electron.*, vol. 35, no. 10, pp. 10238–10248, Oct. 2020, doi: 10.1109/TPEL.2020.2980881.
[97] *Vehicles Boats and Internal Combustion Engines–Radio Disturbance Characteristics–Limits and Methods of Measurement for the Protection of On-Board Receivers*, Standard CISPR 25, 2016.
[98] A. K. Morya, M. C. Gardner, B. Anvari, L. Liu, A. G. Yepes, J. Doval-Gandoy, and H. A. Toliyat, "Wide bandgap devices in AC electric drives: Opportunities and challenges," *IEEE Trans. Transport. Electrific.*, vol. 5, no. 1, pp. 3–20, Mar. 2019, doi: 10.1109/TTE.2019.2892807.
[99] M. Yang, Z. Lyu, D. Xu, J. Long, S. Shang, P. Wang, and D. Xu, "Resonance suppression and EMI reduction of GaN-based motor drive with sine wave filter," *IEEE Trans. Ind. Appl.*, vol. 56, no. 3, pp. 2741–2751, May 2020, doi: 10.1109/TIA.2020.2969873.
[100] C. T. Morris, D. Han, and B. Sarlioglu, "Comparison and evaluation of common mode EMI filter topologies for GaN-based motor drive systems," in *Proc. IEEE Appl. Power Electron. Conf. Expo. (APEC)*, Mar. 2016, pp. 2950–2956, doi: 10.1109/APEC.2016.7468282.
[101] D. Han, S. Li, Y. Wu, W. Choi, and B. Sarlioglu, "Comparative analysis on conducted CM EMI emission of motor drives: WBG versus Si devices," *IEEE Trans. Ind. Electron.*, vol. 64, no. 10, pp. 8353–8363, Oct. 2017, doi: 10.1109/TIE.2017.2681968.
[102] A. M. Hava and E. Ün, "A high-performance PWM algorithm for common-mode voltage reduction in three-phase voltage source inverters," *IEEE Trans. Power Electron.*, vol. 26, no. 7, pp. 1998–2008, Jul. 2011, doi: 10.1109/TPEL.2010.2100100.
[103] Y. Huang, J. Walden, A. Foote, H. Bai, D. Lu, F. Jin, and B. Cheng, "Analytical characterization of CM and DM performance of three-phase voltage-source inverters under various PWM patterns," *IEEE Trans. Power Electron.*, vol. 36, no. 4, pp. 4091–4104, Apr. 2021, doi: 10.1109/tpel.2020.3024836.
[104] Y. Sukhatme, J. Titus, P. Nayak, and K. Hatua, "Digitally controlled active gate driver for SiC MOSFET based induction motor drive switching at 100 kHz," in *Proc. IEEE Transp. Electrific. Conf. (ITEC-India)*, Dec. 2017, pp. 1–5, doi: 10.1109/ITEC-India.2017.8356953.
[105] J.-L. Kotny, T. Duquesne, and N. Idir, "Influence of temperature on the EMI filter efficiency for embedded SiC power converters," in *Proc. IEEE Vehicle Power Propuls. Conf. (VPPC)*, Dec. 2017, pp. 1–6, doi: 10.1109/VPPC.2017.8330890.
[106] F. Hami, H. Boulzazen, and M. Kadi, "High-frequency characterization and modeling of EMI filters under temperature variations," *IEEE Trans. Electromagn. Compat.*, vol. 59, no. 6, pp. 1906–1915, Dec. 2017, doi: 10.1109/TEMC.2017.2679700.
[107] B. Narayanasamy, H. Peng, Z. Yuan, A. I. Emon, and F. Luo, "Modeling and analysis of a differential mode active EMI filter with an analog twin circuit," *IEEE Trans. Electromagn. Compat.*, vol. 62, no. 4, pp. 1591–1600, Aug. 2020, doi: 10.1109/TEMC.2020.3006427.

ZELIANG ZHANG was born in Shaanxi, China, in 1995. He received the B.S. and M.S. degrees in electrical engineering from Northwestern Polytechnical University (NPU), Xi'an, China, in 2017 and 2020, respectively. He is currently pursuing the Ph.D. degree with the University of York.

His research interests include motor drives, electromagnetic interference, and fault diagnosis.

YIHUA HU (Senior Member, IEEE) received the B.S. degree in electrical motor drives and the Ph.D. degree in power electronics and drives from the China University of Mining and Technology, Beijing, China, in 2003 and 2011, respectively.

From 2011 to 2013, he was with the College of Electrical Engineering, Zhejiang University, as a Postdoctoral Fellow. From 2013 to 2015, he was a Research Associate with the Power Electronics and Motor Drive Group, University of Strathclyde. He is a currently a Reader with the Department of Electrical Engineering and Electronics, University of York. His research interests include renewable generation, power electronics converters and control, electric vehicle, more electric ship/aircraft, smart energy systems, and nondestructive test technology.

Dr. Hu is a Fellow of IET and an Associate Editor of the *IET Renewable Power Generation*, *IET Intelligent Transport Systems*, and *Power Electronics and Drives*.

XIAO CHEN (Member, IEEE) received the B.Eng. degree from the Harbin Institute of Technology, Weihai, China, in 2009, the M.Eng. degree from the Harbin Institute of Technology, Harbin, China, in 2011, and the Ph.D. degree from The University of Sheffield, Sheffield, U.K., in 2015, all in electrical engineering.

He is currently a Research Associate with the Department of Electronic and Electrical Engineering, The University of Sheffield. His current research interest includes the modeling, design, and analysis of permanent-magnet synchronous machines for traction applications.

GERAINT WYN JEWELL received the B.Eng. and Ph.D. degrees in electrical engineering from The University of Sheffield, Sheffield, U.K., in 1988 and 1992, respectively.

Since 1994, he has been a member of Academic Staff with the Department of Electronic and Electrical Engineering, The University of Sheffield, where he is currently a Professor of Electrical Engineering, the Head of Department, and the Director of the Rolls-Royce University Technology Centre in Advanced Electrical Machines. He is also a Research Associate with the Department of Electronic and Electrical Engineering, The University of Sheffield. His current research interest includes the modeling, design, and analysis of permanent-magnet synchronous machines for traction applications.

HONG LI (Senior Member, IEEE) received the B.Sc. degree from the Taiyuan University of Technology, Taiyuan, China, in 2002, the M.Sc. degree from the South China University of Technology, Guangzhou, China, in 2005, and the Ph.D. degree from Fernuniversität, Hagen, Germany, in 2009, all in electrical engineering.

She is currently a Full Professor with the School of Electrical Engineering, Beijing Jiaotong University, Beijing, China. She has authored/coauthored one book, 36 journal articles, and 45 conference papers. She has also authorized 24 patents. Her research interests include nonlinear modeling, analysis and its applications, EMI suppressing methods for power electronic systems, and wide bandgap power devices and applications.

Prof. Li is an Associate Editor of the IEEE TRANSACTIONS ON INDUSTRIAL ELECTRONICS, the IEEE OPEN JOURNAL OF INDUSTRIAL ELECTRONICS SOCIETY, and the *Chinese Journal of Electrical Engineering*, and the Vice Chairman of the Electromagnetic Compatibility Specialized Committee in China Power Supply Society.